Exchange bias in (FeNi/IrMn)*n* multilayer films evaluated by static and dynamic techniques

2014 J. Phys. D: Appl. Phys. 47 255002

(http://iopscience.iop.org/0022-3727/47/25/255002)

IOP Publishing Journal of Physics D: Applied Physics

J. Phys. D: Appl. Phys. **47** (2014) 255002 (8pp) doi:10.1088/0022-3727/47/25/255002

Exchange bias in (FeNi/IrMn)$_n$ multilayer films evaluated by static and dynamic techniques

Shankar Khanal[1,2], Andrei Diaconu[1,2], Jose M Vargas[1,5], Denny R Lenormand[1,2], Carlos Garcia[3], C A Ross[4] and Leonard Spinu[1,2]

[1] Advanced Materials Research Institute, University of New Orleans, New Orleans, LA 70148, USA
[2] Department of Physics, University of New Orleans, New Orleans, LA 70148, USA
[3] Departamento de Fisica, Universidad Técnica Federico Santa María, Valparaiso, Chile
[4] Department of Materials Science and Engineering, Massachusetts Institute of Technology, Cambridge, MA, USA

E-mail: LSpinu@uno.edu

Received 9 February 2014, revised 24 April 2014
Accepted for publication 3 May 2014
Published 30 May 2014

Abstract

Exchange bias properties of [FeNi/IrMn]$_n$ multilayer films with variable thickness of the ferromagnetic layers and different repetitions n were determined by using static and dynamic measurement techniques. The static magnetic properties were revealed through magnetometry measurements at room temperature following major hysteresis loops and first-order reversal curves protocols. Room temperature x-band ferromagnetic resonance (FMR) and vector network analyser (VNA)-FMR experiments were used to determine dynamically the exchange anisotropy in the FeNi/IrMn multilayers. From the static measurements the exchange anisotropy was determined while dynamic measurements allowed the determination of additional parameters including anisotropy field, saturation magnetization and rotatable anisotropy. The differences between the values of the exchange biased obtained from each technique are discussed.

Keywords: exchange bias, multilayers, ferromagnetic resonance, first-order reversal curves

(Some figures may appear in colour only in the online journal)

1. Introduction

Thin-film ferromagnetic (F) multilayer systems, where at least one antiferromagnetic (AF) layer is intercalated between F layers, are an important class of exchange-coupled magnetic nanostructured materials [1–3]. The structural imperfections, such as interface roughness, interdiffusion, grain boundaries and reduced coordination number at the interface further frustrate and pin the exchange-coupled F/AF layers, and new phenomena arise in these systems which makes them ideal candidates for technological applications such as spin-valve-based sensors for hard disks [4–6] and microwave devices in the gigahertz range [7–9]. For the above-mentioned applications as well as for fundamental studies of magnetic interactions and magnetization reversal processes, a particularly useful configuration is a periodic array of thin F layers where the thickness of the F and AF components can be controlled.

In previous studies samples with variable thicknesses of the F and/or AF layers were considered. Regarding the thickness effect of the AF layer, Choi *et al* [10] examined the dependence of magnetic anisotropies of the exchange-biased FeNi/FeMn/CoFe films using angular dependent ferromagnetic resonance (FMR) experiments; a misalignment between the uniaxial and unidirectional anisotropies could be observed which was dependent on the thickness of the AF layer. The AF-layer thickness dependence of the anisotropy misalignment was explained by the contributions from thickness-dependent AF anisotropy and spin frustration

[5] Present address: Centro Atomico Bariloche, 8400 S.C. de Bariloche, RN, Argentina.

at F/AF interfaces due to structural imperfections. Phuoc *et al* [11] performed a detailed characterization of the magnetic and microwave properties between 1 and 4 GHz of FeNi/FeMn multilayer films with different thicknesses of the Permalloy layers. A multimodal FMR absorption was observed, which was interpreted in terms of the different exchange interfacial energies acting on each layer. Several exchange-biased FeNi/IrMn multilayer systems with different thickness of the F layers and layer repetition number were studied by magnetoimpedance (MI) experiments for frequencies up to 3 GHz [12, 13]. The MI response and its dependence of the variable exchange bias as provided by the varying thickness of the F layer was explained in terms of a coherent rotation model including an exchange bias energy term.

In spite of intense studies triggered by the technological and fundamental importance of exchange-biased structures a correlation between their static and dynamic magnetic properties is still lacking. In this work we present a comprehensive study of both the static and dynamic magnetic response of $[FeNi/IrMn]_n$ exchange-biased multilayers films with variable thickness of the F layers. The static magnetic properties are revealed through magnetometry measurements at room temperature following major hysteresis loops (MHL) and first-order reversal curves (FORC) protocols. As shown previously [14, 15] the FORC method provides more information about magnetization reversal, including distributions of coercive and interaction fields, than MHL from which one can obtain only the exchange bias and coercive field values. As we will show, the supplementary information provided by FORC diagrams is essential in correlating the observed exchange bias phenomena with sample characteristics such as inherent inhomogeneities existing at the AF/F interfaces. The dynamic response is examined at room temperature through X-band and vector network analyser (VNA)-FMR experiments with frequencies up to 25 GHz. Analysing the exchange bias properties at different frequencies provides additional insight into the interfacial properties of the AF and F layers forming the multilayer samples. The observed decrease of the exchange bias field with the increase of the FMR frequency is consistent with previously reported X-band (9.65 GHz) and Q-band (34.0 GHz) FMR experiments performed at room temperature for polycrystalline $Ni_{81}Fe_{19}$ coupled to NiO [17].

2. Experimental

Rectangular slabs of 3×12 mm silicon wafer thermally oxidized with 50 nm SiO_2 were used as substrate. Multilayer films of composition [FeNi (t nm)/IrMn (20 nm)] $\times\, n(t)$ where FeNi represents Ni (80 at%) Fe (20 at%), were deposited at room temperature using dc-triode sputtering with a base pressure of 3.0×10^{-9} Torr and an Ar pressure of 1.0×10^{-3} Torr. A 10 nm thick Ti layer was used as both a seed layer and a capping layer for the multilayers. A magnetic field of 250 Oe was applied during deposition along the long axis of the strips in order to induce a longitudinal magnetic anisotropy. Thickness, t, and number of repetitions, $n(t)$, are given by $t = 20$ nm, 60 nm, 80 nm; $n = 10, 5, 4$, respectively.

Table 1. Structural information of the samples S_1, S_2 and S_3 deposited at room temperature using dc-triode sputtering.

Sample	FeNi t (nm)	IrMn t (nm)	Repetition number, n	Full thickness (nm)
S_1	20	20	10	400
S_2	60	20	5	400
S_3	80	20	4	400

The number of repetitions and thicknesses were fixed in such a way that the total thickness of all the samples was kept the same. As reported elsewhere [13], a linear response of the MI at zero field can be achieved in these samples which is advantageous for sensor applications. Due to the fabrication process, the three samples showed strong in-plane anisotropy, with unidirectional exchange bias field at room temperature. A summary of the samples is presented in table 1.

The MHL and FORC measurements were conducted at room temperature on a Princeton AGM-VSM magnetometer using the VSM option. This instrument is able to record a set of 100 FORCs in less than 2 h, with a typical sensitivity of 0.5 μemu and 1 s average time per point. In all MHL and FORC experiments the applied field was applied along the easy axis of the samples.

The X-band FMR measurements were performed at room temperature using a Bruker EMX FMR spectrometer operating at 9.87 GHz (X-band). The FMR experiments were performed with the magnetic field driven from $H = 0$ Oe to 13 kOe in ~80 s sweeping time (163 Oe s^{-1}). The angle-dependent FMR experiments were carried out for each sample with an angle step of $\Delta\phi_H = 3°$. From the single-line absorption-derivative FMR spectra, two characteristic parameters could be determined, i.e. the resonant field H_{res} as the centre point of the spectrum, and the peak-to-peak line width ΔH_{pp}.

Broadband FMR experiments were carried out at room temperature using a VNA feeding a coplanar waveguide (CPW) with the multilayer samples positioned on top of the CPW. The experimental setup has been optimized to enable frequency sweeps from 1 up to 25 GHz as the static magnetic field varies between −3.5 and 3.5 kOe. The magnetic field was applied parallel to the axis of the CPW. The microwave signal propagation along the CPW produced a microwave pumping field in-plane with the thin-film sample and perpendicular to the direction of the waveguide. In this condition, the microwave pumping field and the applied magnetic field were kept perpendicular to each other such that the perpendicular FMR pumping configuration was always conserved. For different values of the static magnetic field, H the transmission coefficient S_{21} was recorded as the frequency was swept. Experimental data are represented as a contour plot of the transmission coefficient S_{21} as a function of frequency and external applied field. The darkest regions of the contour plots represent the regions with the lowest transmission of the CPW coupled with the sample, therefore the regions with the highest microwave absorption of the samples. Similar results were obtained with the VNA in continuous wave mode at different fixed frequencies and sweeping the external magnetic field.

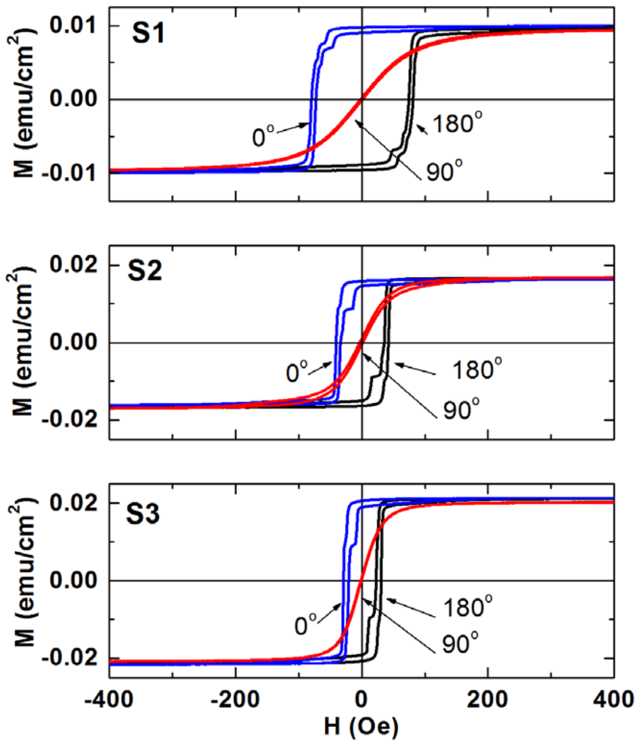

Figure 1. MHL for samples S_1, S_2 and S_3 at different orientations of the applied magnetic field.

3. Results and discussion

3.1. Static magnetic measurements: MHL and FORC

Figure 1 shows the MHLs for all samples for three different in-plane orientations (0°, 90° and 180°) of the applied magnetic field, H. When the magnetic field was applied parallel to the exchange bias field (labelled as 0° orientation), the magnetization loop was shifted towards the negative field axis, whereas when the magnetic field was applied antiparallel (labelled as 180° orientation), the loop was shifted towards the positive field values. The hysteresis loops present no coercivity and passed through the origin for a magnetic field orientation perpendicular to the direction of the exchange bias field (90°).

All samples displayed very similar values of low coercivity H_c (3.5 Oe for S_1 and S_2 and 4.2 Oe for S_3) but very different exchange bias values, depending on the number of repetitions of the AF/F layers. Thus, the exchange bias field H_{eb} for the three samples determined from the MHL measurements as the shift of the hysteresis loops with respect to the origin was 76.0 Oe, 37.0 Oe and 24.8 Oe, for the S_1, S_2, S_3 samples, respectively (see table 2). It is worth mentioning that the change of H_{eb} is related to the thickness of the F layers in each sample. Although the total thickness of the film was constant, the thickness of the FeNi layer changed for each sample. Indeed, as the thickness of the FeNi layer is reduced, the contribution of the interface coupling between F/AF is enhanced, determining an increase of the exchange bias field [16].

Comparing the general shape of the hysteresis loops for the three samples one notices extra steps in the magnetization

Table 2. Parameters obtained from static magnetic measurement.

	MHL		FORC			
Sample	H_{eb} (Oe)	H_c (Oe)	$H_{eb} = \langle h_u \rangle$ (Oe)	$\sigma(h_u)$ (Oe)	$H_c = \langle h_c \rangle$ (Oe)	$\sigma(h_c)$ (Oe)
S_1	76.0	3.5	78.0	6.3	0.7	4.4
S_2	37.0	3.5	39.0	3.4	2.8	3.0
S_3	24.8	4.2	26.0	2.7	4.5	1.8

curves between positive and negative saturation. Two main features of these extra steps can be analysed for each of the samples: their relative magnitude with respect to the saturation magnetization and the number of steps. Concerning the former, one observes that for sample S_3 the relative change in magnetization of the extra step is the largest while for sample S_2 and S_1 these are proportionally smaller. Sample S_3 has four repetitions of the (FeNi)/(IrMn) layers, with the first F layer deposited on the Ti seed layer interacting only with one IrMn layer, while the other three FeNi films in sample S_3 are sandwiched between two layers of IrMn. Consequently, for sample S_3, one F layer out of 4 (25%) will have different magnetic properties from the others. Similarly, one FeNi layer out of 5 (20%) for sample S_2 and one F layer out of 10 (10%) for sample S_1 will have different magnetic properties from the others within the same sample. These values (25%, 20% and 10%) roughly correlate with the magnetization kinks observed for samples S_3, S_2 and S_1, respectively, and can be associated with the influence of the first F layer. Regarding the number of extra steps, for sample S_1 two extra steps are visible whereas for sample S_2 one step is clearly marked and a second one is present as an inflection of the magnetization curve. For sample S_3 only one extra step is noticeable. The number of extra steps observed can be related to the different unidirectional magnetic anisotropies acting on different interfaces of the samples determined presumably by the microstructural defects/roughness of the F/AF interfaces [11, 17]. Sample S_1 composed of 10 repetitions of the FeNi/IrMn layers is expected to show more features in its hysteresis loop compared to samples S_2 and S_3 containing only 5 and 4 repetitions, respectively. A more detailed account of the effect of the inhomogeneities from the AF/F interfaces on the magnetization reversal is given by the FORC method results.

FORCs, introduced first by Mayergoyz [18] as an identification method for the Preisach model, were proposed by Pike [19] as an improved method for studying magnetic interactions in assemblies of magnetic fine particles. Soon after it was proposed, the FORC method became an important experimental approach for studying interaction and switching mechanisms in hysteretic systems for a wide class of different materials ranging from magnetic [14, 20–23] and electric [24] to spin transition systems [25].

The FORC measurement begins with a positive saturation of the samples followed by a ramping down of the applied field to a reversal field H_R. Then the field is increased again up to saturation and magnetization is measured at different values of the applied field H. Thus, for different values of the reversal field H_R a family of FORCs is obtained with $M(H, H_R)$

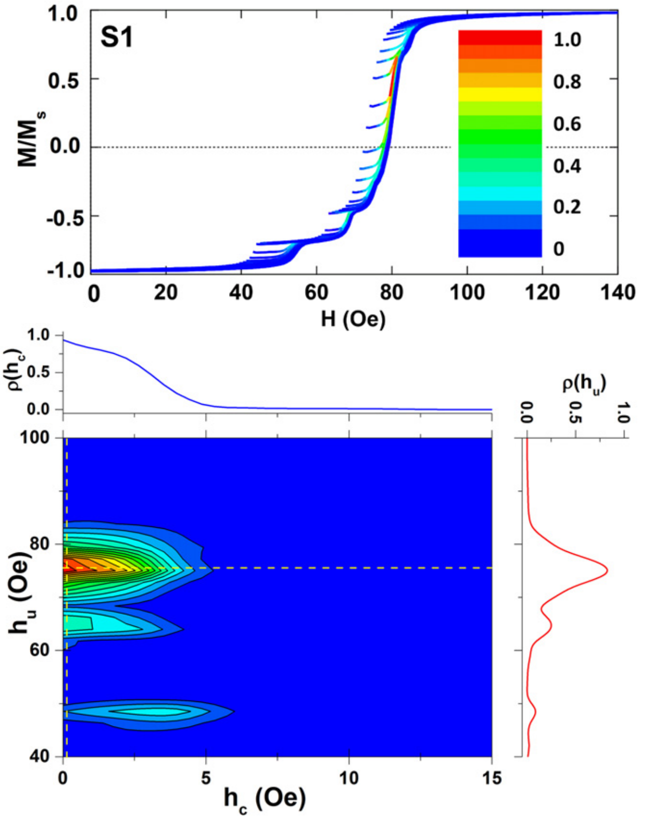

Figure 2. FORC (top) and FORC diagram (bottom) in the coordinates (h_c, h_u) for sample S_1. The top and the side insets for bottom figure represent the coercive field and interaction field distribution profiles obtained at the location of the horizontal and vertical dotted lines, respectively.

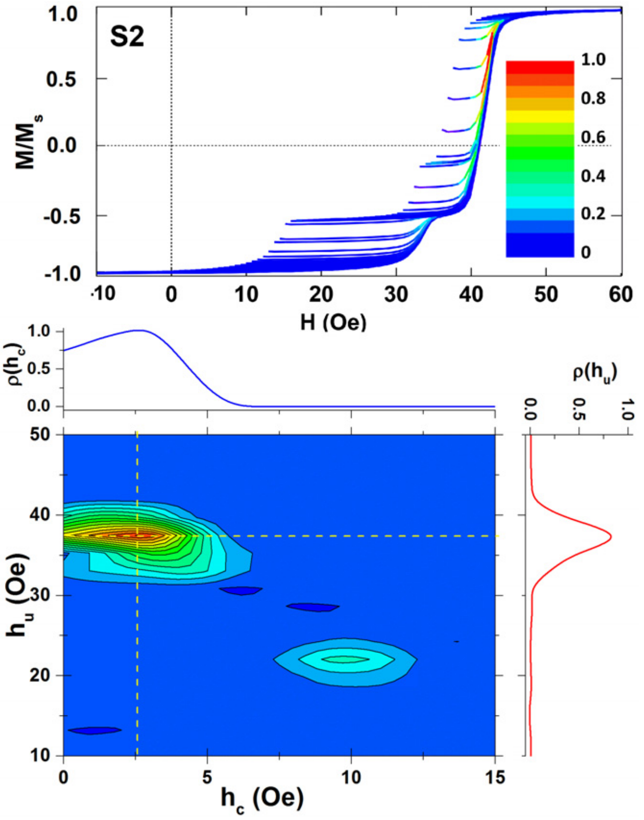

Figure 3. FORC (top) and FORC diagram (bottom) in the coordinates (h_c, h_u) for sample S_2. The top and the side insets for bottom figure represent the coercive field and interaction field distribution profiles obtained at the location of the horizontal and vertical dotted lines, respectively.

representing the magnetization obtained in the applied field H after a field reversal at H_R. The normalized FORC distributions are obtained by computing the mixed second order derivative of magnetization $M(H, H_R)$ [18, 19]:

$$\rho(H, H_R) = -\frac{1}{2M_S}\frac{\partial^2 M(H, H_R)}{\partial H_R \partial H} \quad (1)$$

where M_S is the saturation magnetization of the sample.

The FORC distributions and diagrams (the contour plots of the FORC distributions) were produced using FORCinel, an algorithm using locally weighted regression smoothing [26]. Usually a new set of coordinates in terms of local coercivity (h_c) and bias (h_u) are defined by $h_c = (H - H_R)/2$ and $h_u = (H + H_R)/2$, which rotates the FORC distribution by 45°. As shown previously, the FORC distribution is very sensitive to distributions of magnetic properties and irreversible switching processes [22], which makes the FORC method suitable for a more detailed analysis of the exchange bias phenomenon than the MHL.

The FORC diagrams represented as 2D contour plot in rotated coordinates (h_c, h_u) for samples S_1, S_2 and S_3 are shown in figures 2, 3 and 4, respectively. In the same figures, top panels display the $M(H, H_R)$ coloured FORCs where in each case the colour is related to the FORC distribution with the legend displayed in each figure. All three samples presented a well-defined main FORC distribution together with additional satellite distributions. The secondary distributions are an indication of the structural inhomogeneities in their respective samples, which are more pronounced in the [FeNi/IrMn] × n samples with higher number n of repetitions. The peak coordinates, (h_c, h_u) of the main FORC distributions located at the intersection of the dotted lines in figures 2–4, provide the coercivity H_c and exchange field H_{eb} values for each sample. Thus, one observes that sample S_1 with the highest number of the multilayer repetitions had the highest H_{eb} value followed by samples S_2 and S_3.

In order to quantitatively compare the FORC diagrams obtained for each sample, a statistical analysis was done on the profiles of both interaction and coercive field distributions corresponding to the main peaks. Hence, the mean field values of the coercive field, $\langle h_c \rangle$, and interaction field, $\langle h_u \rangle$, and their corresponding standard deviations, $\sigma(h_c)$ and $\sigma(h_u)$, were obtained using a single Gaussian distribution function. The parameters for the three samples are given in table 2.

From the values in table 2 one observes that, as layer number n increased and the FeNi layer thickness decreased, the exchange bias value $H_{eb} = \langle h_u \rangle$ increased, with values consistent with those obtained from MHL measurements. However, FORC provides more insight in the exchange bias phenomenon than MHL showing that as the H_{eb} increased the standard deviations $\sigma(h_c)$ and, $\sigma(h_u)$ of the FORC diagrams increased, confirming the existence of a higher degree of

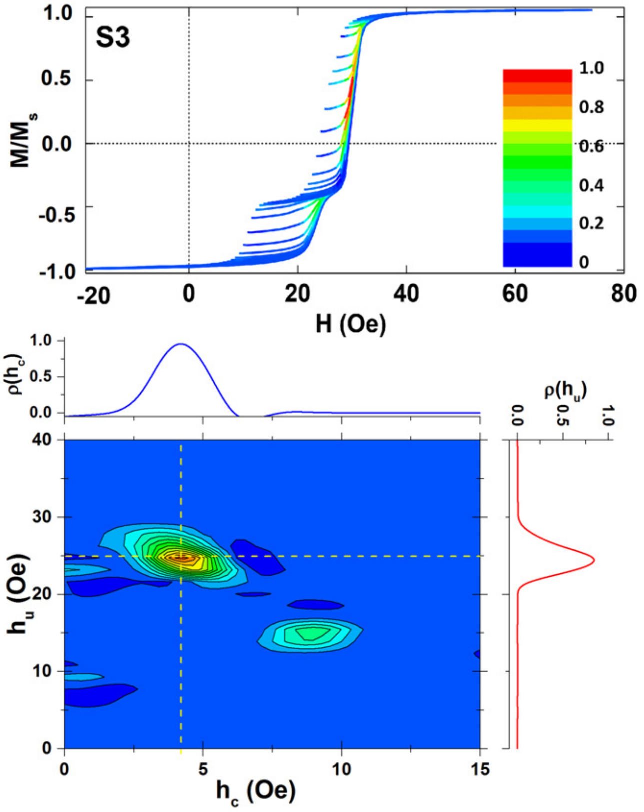

Figure 4. FORC (top) and FORC diagram (bottom) in the coordinates (h_c, h_u) for sample S_3. The top and the side insets for bottom figure represent the coercive field and interaction field distribution profiles obtained at the location of the horizontal and vertical dotted lines, respectively.

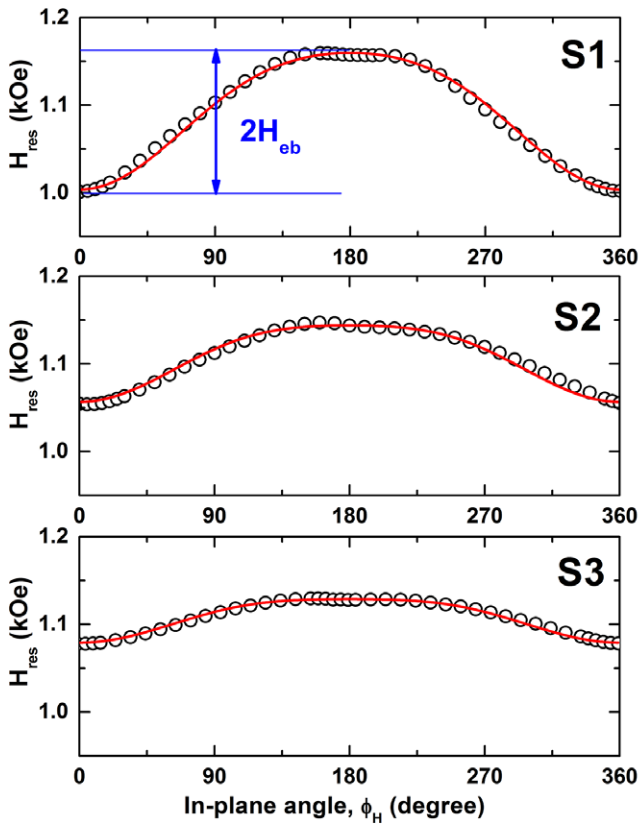

Figure 5. In-plane X-band (9.87 GHz) FMR angular variation spectra measured for the three samples. The superimposed continuous lines correspond to the fit using the equation (2).

inhomogeneity in the samples with high number of the F/AF interfaces. Moreover, the values of the coercive fields as determined from FORC, $H_c = \langle h_c \rangle$, were slightly different from those determined from MHL measurements, especially for samples S_1 and S_2.This is due to the fact that the values in table 2 are obtained from the fit of the main FORC distributions for each sample without taking into account the contribution from the satellite distributions, more present in samples S_1 and S_2.

3.2. Dynamic measurements: X-band and broadband FMR

FMR is a dynamic perturbative measurement involving small variations of magnetization around equilibrium and characterizes the free energy of the system in the vicinity of energy minima. As the free energy is dependent on the exchange coupling, the study of the FMR line shape and its angular variation provide useful microscopic information about exchange bias field H_{eb} and other internal and demagnetization field effects [27–29]. FMR of multilayer samples is sensitive to the magnetization at the interface of the F layer, and therefore it is possible to deduce information concerning the abruptness of the interface and the magnetization profile in its vicinity as well [27].

The in-plane angular variation of the resonance field H_{res} for all three samples is shown in figure 5. The unidirectional anisotropy is clearly reflected in the bell-shaped angular variation of the resonance field. Depending on the reciprocal orientation of the external magnetic field and exchange bias, the resonance field varied from a minimum value, H_{res} (0°) when the fields were parallel, to a maximum value, H_{res} (180°) when the applied magnetic field was antiparallel to the direction of the exchange bias field. From the in-plane angular variation the exchange bias field can be obtained from the difference $[H_{res}(180°) - H_{res}(0°)] = 2H_{eb}$ as shown in figure 5. An asymmetrical fine structure of the angular dependence of the resonance field can be observed, that can be related to the misaligned anisotropy [10] or higher order anisotropy terms [30]. The detailed analysis of this fine structures is beyond the scope of this paper and in the following we use a simple model, which provides information about the anisotropy field, H_K of the F layer obtained from the fit of the expression below giving the overall shift of the in-plane resonance field, H_{res} [27, 31, 32]:

$$\delta H_{res} = H_{res} - H_{res,0} = H_{eb} \cos \phi_H + H_K \cos 2\phi_H \qquad (2)$$

where the first term accounts for the unidirectional anisotropy and the second term takes into account the uniaxial anisotropy of the F layers. The values of the exchange bias and anisotropy fields for all three samples as obtained by fitting the X-band FMR data using equation (2) are given in table 3. A systematic increase of the exchange bias field with the decrease of the thickness of the F layer is observed,

Table 3. Parameters obtained from dynamic magnetic measurements.

	X-band FMR			Broadband FMR			
Sample	H_{eb} (Oe)	H_K (Oe)	$H_{res,0}$ (Oe)	H_{eb} (Oe)	M(emu cm^{-3})	H_K (Oe)	H_{ra} (Oe)
S_1	78.0	10.1	1092	72.3	878	10.1	38.9
S_2	43.6	8.2	1108	35.4	859	8.2	34.3
S_3	24.8	5.1	1109	22.4	875	5.1	37.3

as in the case of static measurements. However, the exchange bias field values obtained from the X-band FMR data are systematically larger than the ones obtained from MHL and FORC measurements, with the largest difference observed for samples S_1 and S_2. This kind of discrepancy between the exchange bias field values obtained from different measurement methods was previously observed for some systems and explained by taking into account the different effect the degree of freedom the antiferromagnet has on reversible and irreversible measurement techniques [33]. MHL and FORC measurements are irreversible measurements involving the irreversible switching of magnetization of the F layer while FMR is a reversible measurement where the magnetization is perturbed by a small amount. From the data presented in table 3 one observes that indeed, the smallest difference between the MHL/FORC and FMR H_{eb} values occurs for sample S_3, with the smallest number of AF layers, and therefore the least affected by the degree of freedom of the AF.

In exchange-biased systems the FMR linewidth was observed to carry interesting information [30]. For our samples, the X-band FMR linewidth was found to mimic the angular variation of the resonance field, with its average values decreasing from sample S_1 to samples S_3. This variation of the FMR linewidth among the studied exchange-biased samples can be correlated with the FORC's distribution of coercive and interaction fields and ultimately with the inhomogeneities existing at the AF/F interfaces. A comprehensive correlation between the FORC data and FMR results including the linewidth, could be made with complementary experimental studies that should include angular dependent FORC experiments.

To get a complete picture of the high frequency response of these exchange bias samples, broadband FMR experiments were conducted using a VNA [29, 34]. Figure 6 shows the contour plot of the transmission coefficient of the CPW coupled with the measured sample as a function of the frequency and applied magnetic field, for sample S_1. The top and right insets display the profiles of the transmitted microwave signal S_{21} versus H at 15 GHz and S_{21} versus f at 2.0 kOe, respectively. The experimental data were fitted using the Kittel formula [34, 35]:

$$f_{res} = \frac{\gamma}{2\pi} \times \sqrt{(H_K + H_{ra} + |H - H_{eb}|)\,(H_K + H_{ra} + |H - H_{eb}| + 4\pi M)} \quad (3)$$

where γ is the gyromagnetic factor and H_{ra} is the rotatable anisotropy field [28, 29]. Rotatable anisotropy field was introduced to include some of the effects of domain-wall

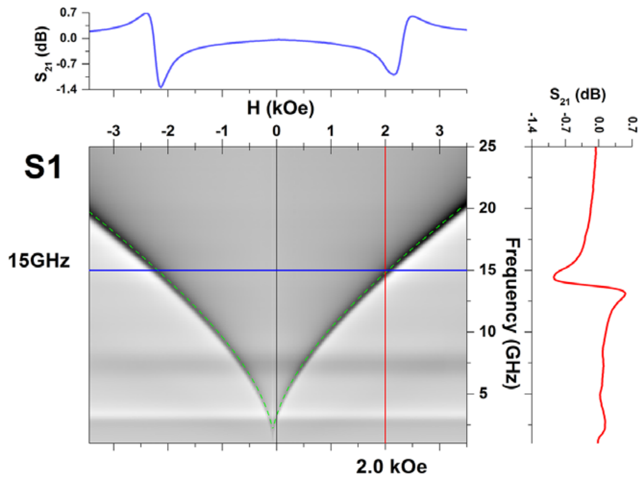

Figure 6. The broadband FMR data plotted as a contour plot of the microwave signal as a function of the microwave frequency and applied magnetic field, for sample S_1. The top and right insets display the profiles of the transmitted microwave signal S_{21} versus H at 15 GHz and S_{21} versus f at 2.0 kOe, respectively.

hysteresis in the antiferromagnet for the interpretation of data obtained with perturbative methods [36]. The easy axis of the rotatable anisotropy follows the macroscopic motion of magnetization direction that minimizes the free energy of the system, having as effect a decrease of the resonance field in all directions. Thus, H_{ra} represents an enhancement of the anisotropy field H_K of the F layer when it is exchange-coupled with an AF layer, and cannot be detected by static magnetic measurement techniques [37]. The fitting procedure provides the values for H_{eb}, M and $H_K + H_{ra}$. The values for H_{ra} are obtained using the values for anisotropy field H_K obtained from the in-plane angular variation of the X-band FMR. Equation (3) fits very well the experimental data with the fitting parameters given in table 3, the fitting curve being represented in figure 6 with a dashed line. Similar good quality fits were obtained for samples S_2 and S_3, with the fitting parameters given in table 3. The exchange bias field values obtained are consistent with the previous results showing the largest value for sample S_1 and smallest for sample S_3, and the values found for the saturation magnetization are in the range of those accepted for Permalloy. The largest value for the rotatable anisotropy was found in sample S_1, with the largest number of F/AF interfaces, supporting the AF origin of H_{ra}.

Comparing the values of the exchange bias obtained from X-band and broadband FMR one observes that the values obtained from broadband FMR are systematically smaller. In average, the frequency of the microwave field in the broadband FMR experiments is larger than in the case of X-band FMR, and a similar effect of decreasing H_{eb} values with the frequency of the FMR was previously observed and explained by relaxation effects of AF grains [38]. The frequency dependent exchange bias indicates the existence of different fractions in the AF part of the interface, with stable and unstable grains. Sample S_3 is the least affected by the contribution of the AF layers, reflected in the smallest difference between the exchange bias field values H_{eb} determined from X-band and broadband FMR. Static and dynamic magnetization experiments allow a comprehensive understanding of the distinctive exchange bias phenomena observed for the three considered samples with different numbers of AF/F interfaces.

4. Conclusions

In summary, the static and dynamic properties of NiFe/IrMn exchange-biased multilayer with different numbers of AF/F interfaces were studied using several experimental techniques. Each measurement method revealed different facets of the exchange bias phenomenon in the studied samples. The shift of the major hysteresis loops provides a simple measurement of the exchange bias. The extra steps in the magnetization curves between positive and negative saturation were associated with the influence of the first ferromagnetic layer and inhomogeneity at the F/AF interfaces. This was confirmed by the FORC measurements where in addition to the main FORC distribution, satellite distributions were observed. The X-band and broadband FMR measurements allowed the investigation of the exchange bias in the dynamic regime and evaluation of additional parameters such as the anisotropy field, saturation magnetization and rotatable anisotropy field.

Acknowledgments

This work was supported by the National Science Foundation, through Grant No ECCS-1028547 and the LASiGMA program under Award No EPS-1003897 with additional support from the Louisiana Board of Regents. CAR acknowledges C-SPIN, one of six STARnet Centers of MARCO and DARPA, and NSF award ECCS1101798. CG acknowledges the financial support from the 7th European Union Framework Programme (FP7-PEOPLE-2012-IRSES, Project No 318901). This research was also supported by Fondecyt Grant No 1140552 and from project 111323 DGIP USM.

References

[1] Nogues J, Sort J, Langlais V, Skumryev V, Surinach S, Munoz J S and Baro M D 2005 Exchange bias in nanostructures *Phys. Rep.* **422** 65–117

[2] Jimenez E, Camarero J, Sort J, Nogues J, Mikuszeit N, Garcia-Martin J M, Hoffmann A, Dieny B and Miranda R 2009 Emergence of noncollinear anisotropies from interfacial magnetic frustration in exchange-bias systems *Phys. Rev.* B **80** 014415

[3] Gong Y, Cevher Z, Ebrahim M, Lou J, Pettiford C, Sun N X and Ren Y H 2009 Determination of magnetic anisotropies, interlayer coupling, and magnetization relaxation in FeCoB/Cr/FeCoB *J. Appl. Phys.* **106** 063916

[4] Sort J, Salazar-Alvarez G, Baro M D, Dieny B, Hoffmann A, Novosad V and Nogues J 2006 Controlling magnetic vortices through exchange bias *Appl. Phys. Lett.* **88** 042502

[5] Sort J, Dieny B and Nogues J 2005 Exchange bias in antiferromagnetic–ferromagnetic–antiferromagnetic structures with out-of-plane magnetization *Phys. Rev.* B **72** 104412

[6] Jimenez E *et al* 2011 Role of anisotropy configuration in exchange-biased systems *J. Appl. Phys.* **109** 07D730

[7] Gloanec M, Rioual S, Lescop B, Zuberek R, Szymczak R, Aleshkevych P and Rouvellou B 2009 Dynamical effect in measurement of the exchange-bias field: a consequence of the slow-relaxer mechanism *Phys. Rev.* B **80** 220404

[8] Dubowik J, Stobiecki F, Goscianska I, Lee Y P, Paetzold A and Roll K 2005 Temperature dependence of ferromagnetic resonance in permalloy/NiO exchange-biased films *Eur. Phys. J.* B **45** 283–8

[9] da Silva R B, Viegas A D C, Nascimento V P, Correa M A, Schelp L F, Baggio-Saitovitch E and Sommer R L 2009 High frequency magnetoimpedance in $Ni_{81}Fe_{19}/Fe_{50}Mn_{50}$ exchange biased multilayer *Appl. Phys. Lett.* **94** 042501

[10] Choi H C, You C Y, Kim K Y, Lee J S, Shim J H and Kim D H 2010 Antiferromagnetic layer thickness dependence of noncollinear uniaxial and unidirectional anisotropies in NiFe/FeMn/CoFe trilayers *Phys. Rev.* B **81** 224410

[11] Phuoc N N, Xu F, Ma Y G and Ong C K 2009 Permalloy–FeMn exchange-biased multilayers grown on flexible substrates for microwave applications *J. Magn. Magn. Mater.* **321** 2685–90

[12] Garcia C, Florez J M, Vargas P and Ross C A 2010 Asymmetrical giant magnetoimpedance in exchange-biased NiFe *Appl. Phys. Lett.* **96** 232501

[13] Garcia C, Florez J M, Vargas P and Ross C A 2011 Effect of the exchange bias coupling strength on the magnetoimpedance of IrMn/NiFe films *J. Appl. Phys.* **109** 07D735

[14] Alonso L, Peixoto T R F and Cornejo D R 2010 Magnetic interaction in exchange-biased bilayers: a first-order reversal curve analysis *J. Phys. D: Appl. Phys.* **43** 465001

[15] Olamit J, Liu K, Li Z P and Schuller I K 2007 Irreversibility of magnetization rotation in exchange biased Fe/epitaxial-FeF_2 thin films *Appl. Phys. Lett.* **90** 032510

[16] Chui K M, Tripathy D and Adeyeye A O 2007 Temperature dependence of magnetotransport properties of $Ni_{80}Fe_{20}/Fe_{50}Mn_{50}/Ni_{80}Fe_{20}$ trilayers *J. Appl. Phys.* **101** 09E512

[17] Phuoc N N and Ong C K 2012 Diluted antiferromagnet effect on magnetic and microwave characteristics of exchange-biased multilayered thin films *J. Appl. Phys.* **111** 093919

[18] Mayergoyz I D 1986 Mathematical-models of hysteresis *IEEE Trans. Magn.* **22** 603–8

[19] Pike C R, Roberts A P and Verosub K L 1999 Characterizing interactions in fine magnetic particle systems using first order reversal curves *J. Appl. Phys.* **85** 6660–7

[20] Roberts A P, Pike C R and Verosub K L 2000 First-order reversal curve diagrams: a new tool for characterizing the magnetic properties of natural samples *J. Geophys. Res.* **105** 28461–75

[21] Spinu L, Stancu A, Radu C, Li F and Wiley J B 2004 Method for magnetic characterization of nanowire structures *IEEE Trans. Magn.* **40** 2116–18

[22] Davies J E, Hellwig O, Fullerton E E, Denbeaux G, Kortright J B and Liu K 2004 Magnetization reversal of Co/Pt multilayers: microscopic origin of high-field magnetic irreversibility *Phys. Rev.* B **70** 224434

[23] Pike C R, Ross C A, Scalettar R T and Zimanyi G 2005 First-order reversal curve diagram analysis of a

perpendicular nickel nanopillar array *Phys. Rev.* B **71** 134407

[24] Stancu A, Ricinschi D, Mitoseriu L, Postolache P and Okuyama M 2003 First-order reversal curves diagrams for the characterization of ferroelectric switching *Appl. Phys. Lett.* **83** 3767–9

[25] Tanasa R, Enachescu C, Stancu A, Linares J, Codjovi E, Varret F and Haasnoot J 2005 First-order reversal curve analysis of spin-transition thermal hysteresis in terms of physical-parameter distributions and their correlations *Phys. Rev.* B **71** 014431

[26] Harrison R J and Feinberg J M 2008 FORCinel: an improved algorithm for calculating first-order reversal curve distributions using locally weighted regression smoothing *Geochem. Geophys. Geosyst.* **9** Q05016

[27] Stoecklein W, Parkin S S P and Scott J C 1988 Ferromagnetic resonance studies of exchange-biased Permalloy thin films *Phys. Rev.* B **38** 6847–55

[28] McMichael R D, Stiles M D, Chen P J and Egelhoff W F 1998 Ferromagnetic resonance studies of NiO-coupled thin films of $Ni_{80}Fe_{20}$ *Phys. Rev.* B **58** 8605–12

[29] Kuanr B K, Maat S, Chandrashekariaih S, Veerakumar V, Camley R E and Celinski Z 2008 Determination of exchange and rotational anisotropies in IrMn/Fe(t)/IrMn exchange coupled structures using dynamic and static techniques: application to microwave devices *J. Appl. Phys.* **103** 07C107

[30] Pechan M J, Bennett D, Teng N C, Leighton C, Nogues J and Schuller I K 2002 Induced anisotropy and positive exchange bias: a temperature, angular, and cooling field study by ferromagnetic resonance *Phys. Rev.* B **65** 064410

[31] Scott J C 1985 Ferromagnetic resonance studies in the bilayer system $Ni_{0.80}Fe_{0.20}/Mn_{0.50}Fe_{0.50}$: exchange anisotropy *J. Appl. Phys.* **57** 3681–3

[32] Layadi A, Cain W C, Lee J W and Artman J O 1987 Investigation of anisotropy by ferromagnetic-resonance (FMR) in exchange-coupled bilayer films *IEEE Trans. Magn.* **23** 2993–5

[33] Xi H W, White R M and Rezende S M 1999 Irreversible and reversible measurements off exchange anisotropy *Phys. Rev.* B **60** 14837–40

[34] Bilzer C, Devolder T, Kim J V, Chappert C, Ruehrig M and Baer L 2009 Dynamics of the exchange field supplied by MnIr layers studied by network analyzer ferromagnetic resonance *J. Appl. Phys.* **106** 063918

[35] Glowinski H, Zaleski K, Sprada J and Dubowik J 2012 Exchange coupled NiFe/NiMn bilayer studied by a vector network analyzer ferromagnetic resonance *Acta Phys. Pol.* A **121** 1145–7

[36] Stiles M D and McMichael R D 1999 Model for exchange bias in polycrystalline ferromagnet–antiferromagnet bilayers *Phys. Rev.* B **59** 3722–33

[37] McCord J, Mattheis R and Elefant D 2004 Dynamic magnetic anisotropy at the onset of exchange bias: the NiFe/IrMn ferromagnet/antiferromagnet system *Phys. Rev.* B **70** 094420

[38] Geshev J, Pereira L G, Schmidt J E, Nagamine L, Saitovitch E B and Pelegrini F 2003 Frequency-dependent exchange bias in NiFe/NiO films *Phys. Rev.* B **67** 1324013